Stability of Vicinal Surfaces: Beyond the Quasistatic Approximation

L. Guin,[1,2] M. E. Jabbour,[1,3] L. Shaabani-Ardali,[4,5] L. Benoit-Maréchal,[1,2] and N. Triantafyllidis[1,3,6]
[1]LMS, École polytechnique, CNRS, Institut polytechnique de Paris, Palaiseau 91128, France
[2]LPICM, École polytechnique, CNRS, Institut polytechnique de Paris, Palaiseau 91128, France
[3]Département de Mécanique, École polytechnique, Palaiseau 91128, France
[4]LadHyX, École polytechnique, CNRS, Institut polytechnique de Paris, Palaiseau 91128, France
[5]DAAA, ONERA, Université Paris-Saclay, Meudon F-92190, France
[6]Aerospace Engineering Department & Mechanical Engineering Department (emeritus), The University of Michigan, Ann Arbor, Michigan 48109-2140, USA

(Received 22 November 2018; revised manuscript received 23 September 2019; published 22 January 2020)

We revisit the step bunching instability without recourse to the quasistatic approximation and show that the stability diagrams are significantly altered, even in the low-deposition regime where it was thought sufficient. In particular, steps are unstable against bunching for attachment-detachment limited growth. By accounting for the dynamics and chemical effects, we can explain the onset of step bunching in Si(111)-(7×7) and GaAs(001) without resort to the inverse Schwoebel barrier or step-edge diffusion. Further, the size-scaling analysis of step-bunch growth, as induced by these two combined effects, agrees with the bunching regime observed at 750 °C in Si(111)-(7×7).

DOI: 10.1103/PhysRevLett.124.036101

Epitaxial crystal growth is often accompanied by changes in surface morphology such as island nucleation and the meandering of atomic steps [1]. A widely observed instability during step-flow growth is step bunching, explained in the early days as a consequence of an inverse Ehrlich-Schwoebel (ES) effect, whereby adatom attachment to descending steps is more favorable than to ascending ones [2,3]. As situations were encountered where the ES effect is either direct or negligible, alternative mechanisms for step bunching were proposed, including the coupling between diffusing species [4,5] and step-edge diffusion [6].

With few exceptions [7–9], the classical stability analyses [3,4,10–15] were carried out in the framework of the quasistatic approximation [1,16,17]. This mathematical simplification is usually considered appropriate in regimes of low deposition rates. In this Letter, we develop a linear stability analysis of the general equations that govern the step dynamics without resorting to this simplification. Surprisingly, we find that the stability predictions are significantly modified, even in the regime of infinitely slow deposition. In addition to challenging the validity of the quasistatic approximation, this result provides a new mechanism for step bunching, which may be pertinent to the understanding of its occurrence in the epitaxial growth of GaAs(001) and Si(111)-(7×7) [18–24].

To study their bunching, steps are assumed straight and, as such, described in a one-dimensional setting by their positions $\{x_n\}_{n\in\mathbb{Z}}$ on the x axis (Fig. 1), with the adatom density on the nth terrace denoted by ρ_n. Letting L_0 be the initial terrace width, D the diffusion coefficient of adatoms on terraces, and ρ^*_{eq} the equilibrium adatom density, we write the equations governing the dynamics of steps in dimensionless form with L_0, L_0^2/D, and ρ^*_{eq} the characteristic length, time, and adatom density, respectively. These consist of the reaction-diffusion equation on each terrace,

$$\partial_t\rho_n = \partial^2_{xx}\rho_n - \bar{\nu}\rho_n + \bar{F}, \tag{1}$$

with $\bar{F} := FL_0^2/(\rho^*_{eq}D)$ and $\bar{\nu} := \nu L_0^2/D$ as the dimensionless counterparts of the deposition rate F and evaporation probability ν, respectively. Equation (1) is supplemented by the step boundary conditions

$$\begin{aligned} -\rho_n^-\dot{x}_{n+1} - (\partial_x\rho_n)^- &= J^-_{n+1},\\ \rho_n^+\dot{x}_n + (\partial_x\rho_n)^+ &= J^+_n, \end{aligned} \tag{2}$$

where the superimposed dot denotes the time derivative and J_n^- and J_n^+ are the dimensionless attachment rates to the nth step from above and below, respectively,

$$\begin{aligned} J_n^- &:= \bar{\kappa}(\rho_{n-1}^- - 1 - \Theta[\![\rho]\!]_{x_n} + f_n),\\ J_n^+ &:= \bar{\kappa}S(\rho_n^+ - 1 - \Theta[\![\rho]\!]_{x_n} + f_n). \end{aligned} \tag{3}$$

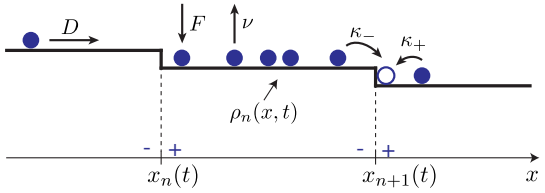

FIG. 1. Schematic of two successive atomic steps displaying the microscopic mechanisms involved in step flow.

 © 2020 American Physical Society

In (3), $[\![\rho]\!]_{x_n} \coloneqq \rho_n(x_n,t) - \rho_{n-1}(x_n,t)$ is the jump in the adatom density at the nth step and, with a as the lattice parameter, $\Theta \coloneqq a^2\rho^*_{eq}$ is the equilibrium adatom coverage. The step kinetics is described by $\bar{\kappa} \coloneqq \kappa_- L_0/D$ and $S \coloneqq \kappa_+/\kappa_-$, where κ_- and κ_+ denote the kinetic coefficients of attachment-detachment (a-d) to descending and ascending steps, respectively. Note that $\bar{\kappa}$ expresses the ratio of a-d kinetics to terrace diffusion kinetics ($\bar{\kappa} \ll 1$ corresponds to a-d limited kinetics and $\bar{\kappa} \gg 1$ to diffusion-limited kinetics), while S specifies the nature of the Ehrlich-Schwoebel effect ($S > 1$ for a direct ES effect and $S < 1$ for an inverse ES effect). The elastic interactions between steps are accounted for by the elastic contribution $f_n \coloneqq -\bar{\alpha}/(x_{n+1}-x_n)^3 + \bar{\alpha}/(x_n - x_{n-1})^3$ to the driving force, defined as the work-conjugate of the step velocity, acting on the nth step. Here, $\bar{\alpha} \coloneqq a^2\alpha/(k_B T L_0^3)$, k_B is the Boltzmann constant, T denotes the absolute temperature, and α gives the magnitude of the dipole-dipole step interactions [17]. Finally, the adatom balance at the nth step yields

$$\dot{x}_n = \Theta(J_n^+ + J_n^-). \tag{4}$$

While we are interested in step bunching as it occurs in the absence of electromigration, the inclusion of the latter, as well as step permeability, in (1)–(4) can be found in Ref. [25]. We refer to $\Theta[\![\rho]\!]$ in (3) as the *chemical effect*. To understand it, recall that (thermal, mechanical or chemical) equilibrium between two phases involves two conditions at their interface: continuity of heat flux and the Gibbs-Thomson relation in thermal equilibrium; continuity of traction and the Maxwell condition in mechanical equilibrium; continuity of both chemical and grand canonical potentials in chemical equilibrium. Since step motion results from the nonequilibrium chemical process of adatom incorporation, it is natural that the jump in the grand canonical potential, which reduces to $\Theta[\![\rho]\!]$ when adatoms behave like an ideal lattice gas, should appear in the driving force at the steps [25–27].

In step-flow models, bunching is investigated through a stability analysis of the fundamental steady-state solution, with equidistant steps $x_n^*(t) = n + V^* t$ propagating with uniform velocity V^* and $\rho_n^*(x,t) = \varrho^*[x - x_n^*(t)]$. Invoking the quasistatic approximation, most existing stability analyses are performed neglecting the dynamics terms, i.e., the *advective* currents $\rho_n^- \dot{x}_{n+1}$ and $\rho_n^+ \dot{x}_n$ in (2) and the *transient* term $\partial_t \rho_n$ in (1). This approximation is usually justified by noting that for sufficiently slow deposition or evaporation the dimensional step velocity, which under deposition is given by FL_0a^2, is small compared with the characteristic diffusion velocity D/L_0. Under deposition, this limit can be expressed by a criterion on the Péclet number [1,16,17],

$$P \coloneqq FL_0^2 a^2/D = \bar{F}\Theta \ll 1. \tag{5}$$

Treatment of the dynamics terms in previous works has been incomplete. In Ref. [7], only the transient term in (1) is accounted for, while in Refs. [14,28,29] only the advective terms are kept in (1)–(4). Reference [9] concerns the limit case of infinitely fast adatom diffusion, leading to an altogether different formulation. Only in Ref. [8] are all the dynamics terms studied, albeit via a stability analysis different from ours and without a systematic investigation of their implications on step bunching. In contrast, in this Letter, we aim at assessing the influence of the dynamics effect under arbitrary conditions of step-flow growth by quantifying its importance with respect to the other stabilizing or destabilizing mechanisms. Specifically, making use of the stability methods of hydrodynamics [30], we perform a linear stability analysis of (1)–(4) without neglecting the dynamics terms. In doing so, we show that their effect on stability is not only major at relatively high deposition rates but is also important in the limit of infinitely slow deposition.

The principal solution is obtained by solving (1)–(4) for V^* and ϱ^*. When perturbing $\{x_n, \rho_n\}_{n\in\mathbb{Z}}$ about the principal solution, (1)–(4) form a free-boundary problem with moving interfaces at $\{x_n\}_{n\in\mathbb{Z}}$. We make the change of spatial variable from x to $u = g_n(x,t) \coloneqq (x - x_n(t))/(x_{n+1}(t) - x_n(t))$ that maps the time-dependent terrace $(x_n(t), x_{n+1}(t))$ into (0,1) and recast the adatom density as

$$\tilde{\rho}_n(u,t) \coloneqq \rho_n(g_n^{-1}(u,t), t), \tag{6}$$

defined, for all n, on $(0,1)\times\mathbb{R}^+$. Rewriting (1)–(4) in terms of the variables $(x_n, \tilde{\rho}_n)$ and linearizing the resulting equations about the principal solution, we obtain a perturbation equation for $\mathbf{q}_n(u,t) \coloneqq (\delta x_n(t), \delta\tilde{\rho}_n(u,t))$, which has the abstract form

$$\mathcal{A}(\mathbf{q}_{n-1}, \mathbf{q}_n, \mathbf{q}_{n+1}, \mathbf{q}_{n+2}) = \mathcal{B}(\partial_t \mathbf{q}_n, \partial_t \mathbf{q}_{n+1}). \tag{7}$$

The operators $\mathcal{A}$ and $\mathcal{B}$ being linear, time independent, and invariant with respect to one-terrace translations, the solution of (7) can be sought as a combination of *Floquet modes*, whose component of wave number $k \in (-\pi, \pi)$ reads

$$\begin{aligned} \delta x_n(t) &= \delta\hat{x}\exp(ikn + \lambda t), \\ \delta\tilde{\rho}_n(u,t) &= \delta\hat{\rho}(u)\exp(ikn + \lambda t), \end{aligned} \tag{8}$$

with λ as the unknown (complex) growth rate associated with k. Inserting (8) in (7) yields, for a given wave number k, a generalized eigenvalue problem of the form

$$\hat{\mathcal{A}}_k \hat{\mathbf{q}} = \lambda \hat{\mathcal{B}}_k \hat{\mathbf{q}}, \tag{9}$$

where $\hat{\mathbf{q}}(u) \coloneqq (\delta\hat{x}, \delta\hat{\rho}(u))$ and $\hat{\mathcal{A}}_k$ and $\hat{\mathcal{B}}_k$ are linear operators deriving from $\mathcal{A}$ and $\mathcal{B}$ (see the Supplemental Material [44] for the full expressions of $\mathcal{A}$, $\mathcal{B}$, $\hat{\mathcal{A}}_k$, and $\hat{\mathcal{B}}_k$). Solving

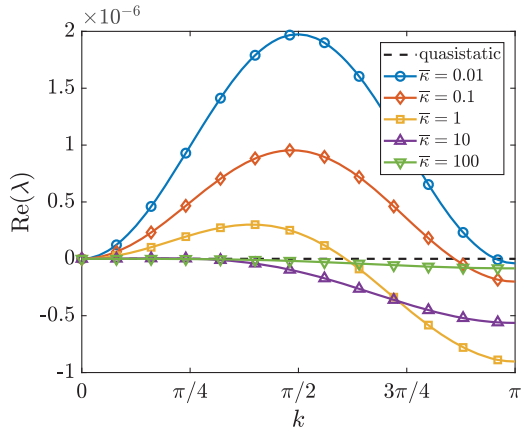

FIG. 2. Dispersion curves giving the critical growth rate $\mathrm{Re}(\lambda)$ as a function of the wave number k under pure deposition ($\bar{\nu} = 0$), for $\bar{F} = 10^{-2}$ and $\Theta = 0.01$. The dotted line indicates neutral stability under the quasistatic approximation and the continuous (colored) lines show the stability results when the dynamics terms are included.

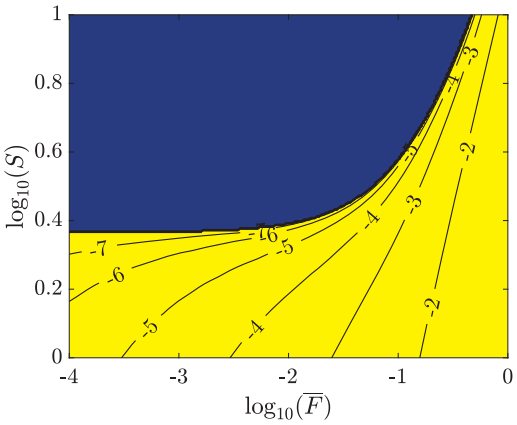

FIG. 3. Stability diagram under deposition ($\bar{\nu} = 0$) in the presence of the ES effect and dynamics, with $\bar{\kappa} = 0.1$ and $\Theta = 0.2$. The stable domain [$\max_{k\in(-\pi,\pi)}\mathrm{Re}(\lambda) < 0$] is shown in blue (dark) and the unstable region [$\max_{k\in(-\pi,\pi)}\mathrm{Re}(\lambda) > 0$] appears in yellow (light). In the latter, isolines display $\max_{k\in(-\pi,\pi)}\log_{10}\mathrm{Re}(\lambda)$, indicating the magnitude of the most critical growth rate. For comparison, the diagram corresponding to the quasistatic approximation (i.e., with only the ES effect) is stable everywhere.

(9) numerically by means of Chebychev spectral methods [31], we obtain for a given k a set of eingenmodes $\hat{\mathbf{q}}$ and associated eigenvalues λ, among which the maximum of $\mathrm{Re}(\lambda)$ provides the critical growth rate of mode k. Steps are stable against bunching if, for any mode k, $\mathrm{Re}(\lambda)[k] \leq 0$.

To study the effect on stability of the dynamics terms *per se*, we "disable" the other mechanisms by setting formally $S = 1$ (symmetric *a-d*), $\Theta[\![\rho]\!] = 0$ (no chemical interactions between steps), and $\bar{\alpha} = 0$ (no elastic interactions). The resulting dispersion relation is shown in Fig. 2, the relevant parameter that determines the influence of the dynamics on stability being $\bar{\kappa}$. Under deposition, the dynamics effect is destabilizing for $\bar{\kappa} < 1$ (approaching the *a-d* limited regime) and stabilizing for $\bar{\kappa} > 1$ (approaching the diffusion-limited regime). Further, the analysis of the dependence of $\mathrm{Re}(\lambda)[k]$ on $\bar{F}$ and Θ shows that the dispersion curve scales linearly with $\bar{F}$ and quadratically with Θ [25]. While the first scaling is shared with the other kinetic mechanisms (ES barrier and chemical effect), the scaling with Θ^2 is common with the chemical effect only, the ES effect and elasticity scaling linearly with Θ. Hence, the impact of both the chemical and dynamics effects is particularly important for materials with relatively high equilibrium adatom coverage.

As noted, the effect of dynamics on stability scales linearly with $\bar{F}$, as do the ES and chemical effects. Therefore, even by taking the limit of infinitely slow deposition rate $\bar{F} \to 0$ (which is equivalent, for a given Θ, to an infinitely small Péclet number) the influence of the dynamics, compared to the other mechanisms, does not become negligible, thus invalidating the quasistatic approximation. Next, we illustrate the breakdown of the quasistatic approximation by showing (Fig. 3) how the dynamics competes with the well-known stabilizing ES effect to destabilize steps against bunching. Although we neglect, for the purpose of the demonstration, the elastic interactions between steps ($\bar{\alpha} = 0$) and the chemical interactions between terraces ($\Theta[\![\rho]\!] = 0$), the stability diagram of Fig. 3 corresponds to physically relevant ranges of S and $\bar{F}$. Moreover, $\Theta = 0.2$ corresponds to typical relatively high values of adatom coverage [as measured, e.g., in GaAs(001) [32,33]] and $\bar{\kappa} = 0.1$ is taken as an illustrative value of the attachment-detachment dominated kinetics, for which the dynamics is destabilizing. Figure 3 illustrates that even for infinitely small Péclet number, the destabilizing effect of the dynamics remains, for a sufficiently small S, prevalent over the stabilizing ES effect.

The quasistatic stability predictions for various step models found in the literature turn out to be significantly modified when the dynamics terms are included. In particular, we now illustrate how these modifications provide possible explanations of experimental observations of the bunching of steps during growth of Si(111)-(7×7) [24] and GaAs(001) [18–23] in the temperature ranges of 700–780 °C and 600–700 °C, respectively.

Within the classical step-flow model, which includes neither the chemical nor the dynamics effects, the only way to account for bunching under growth is to invoke an inverse ES effect. However, studies on Si(111)-(7×7), based on observations of denuded zones around steps [34,35], the decay rates of islands and holes [36], and the distributions of island nucleations [37], lead to contradictory interpretations, namely a direct [36], inverse [35,37], and neutral Schwoebel barrier [34]. On the other hand, it was concluded from work on the growth of mounds [38] that the ES barrier is weakly direct in GaAs(001). Given the limited evidence of an inverse

Schwoebel effect, in order to explain step bunching, new physical mechanisms—which are plausible but without clear evidence of their existence—have been proposed, such as the coupling between diffusing species [4,5] during vapor phase epitaxy of GaAs or step edge diffusion [6] in molecular beam epitaxy of Si(111).

Without resort to these additional mechanisms, we show how accounting for the chemical and dynamics effects can lead to unstable crystal growth. To this end, with estimations of the physical parameters obtained from the experimental literature, we quantify how these effects compete with the stabilizing elastic interactions and ES effect.

For Si(111)-(7×7), given the conflicting evidence of the Schwoebel effect, we assume symmetric attachment-detachment ($S=1$). The coefficient $\bar{\alpha}$ for dipole-dipole interactions is obtained from atomistic computations [39] and is typically $\bar{\alpha}=5\times 10^{-5}$ for $L_0=20$ nm. With no estimations of $\bar{\kappa}$, we take a range that accounts for all possible regimes, from *a-d* limited kinetics ($\bar{\kappa}\ll 1$) to diffusion-limited kinetics ($\bar{\kappa}\gg 1$). Similarly, given the lack of data on D, estimation of $\bar{F}$ is difficult. Thus, we cover four decades below the typical upper bound of step flow growth $\bar{F}=1$. Finally, we take $\Theta=0.01$ for the equilibrium adatom coverage, a low value, which tends to underestimate the influence of the dynamics and chemical effects. We see on the stability diagram (Fig. 4) for the deposition of Si(111)-(7×7) that, as a result of the destabilizing chemical and dynamics effects, there exists a large unstable domain. Further, noting that in terms of dimensionless units the time needed for the deposition of one monolayer is $1/P$, in the region $\bar{\kappa}<10^{-1}$, the typical number of monolayers for the instability to develop is 50 to 100. Hence, with observations [24] that the instability occurs between 30 and 300 monolayers, the mechanisms considered herein are sufficiently fast to explain step bunching in the experiments under consideration.

The plausible implication of the chemical and dynamics effects in the step bunching of GaAs(001) is also confirmed quantitatively. For this material, the elastic interactions are weaker ($\bar{\alpha}=5\times 10^{-6}$ for $L_0=16$ nm associated with a miscut angle of 1° [40,41]), and Krug suggests in Ref. [38] the existence of a direct ES effect whose strength, estimated from an energetic barrier, is roughly $S=2$. Moreover, measurements of the equilibrium adatom coverage in GaAs(001) show that it is in the high range, $\Theta=0.2$ [32,33]. Finally, from the knowledge of the deposition rates in the experiments considered in Refs. [18–23] combined with measurements of the diffusion coefficient D of GaAs(001) [42,43], we estimate that $\bar{F}$ is between $\bar{F}=10^{-2}$ and $\bar{F}=1$. With these parameters, while both elastic interactions and the Schwoebel barrier are stabilizing, the entire domain $10^{-2}<\bar{\kappa}<10^{2}$ and $10^{-2}<\bar{F}<1$ is unstable (see the Supplemental Material [44] for a discussion of the corresponding stability diagram).

Finally, we numerically solve the nonlinear moving boundary problem whose linearization yields (1)–(4), cf. the Supplemental Material [44]. First noting that our simulations confirm the development of bunching under the combined dynamics and chemical effects, we perform size-scaling analyses on the patterns of the step bunches [45–47] to identify from the experiments of Omi *et al.* on Si(111) the bunching regime(s) consistent with the dynamics and chemical effects. To this end, we obtain from the evolution of the bunch height BH and surface roughness

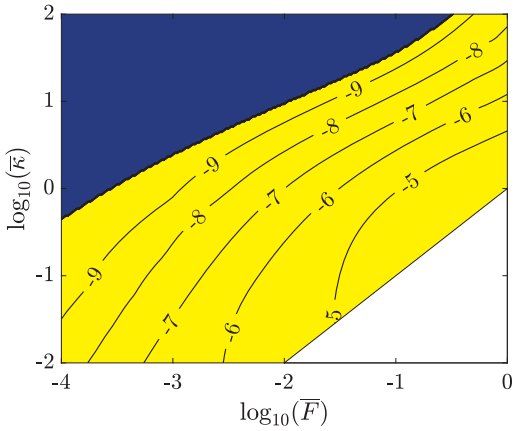

FIG. 4. Stability diagram for the deposition of Si(111)-(7×7), with $\bar{\nu}=0$, $\Theta=0.01$, $S=1$, and $\bar{\alpha}=5\times 10^{-5}$. Blue (dark) and yellow (light) correspond to the stable and unstable domains, respectively, and isolines display $\max_{k\in(-\pi,\pi)}\log_{10}\mathrm{Re}(\lambda)$. The white area corresponds to an unphysical domain where the adatom density reaches values well above the equilibrium adatom coverage.

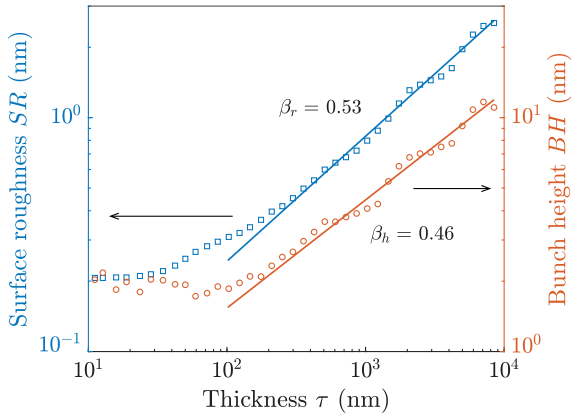

FIG. 5. Evolution of the median bunch height and surface roughness with the deposited thickness, obtained from simulations of the nonlinear moving boundary problem accounting for the combined dynamics-chemical effect, with $\bar{F}=10^{-3}$, $\bar{\kappa}=10^{-2}$, $\Theta=2\times 10^{-2}$, $S=1$, and $\bar{\alpha}=2\times 10^{-7}$. Since the early transient phase corresponds to step pairing, the linear fitting that yields β_h and β_r is performed on the subsequent bunch-growth phase.

SR with the deposited thickness τ the exponents β_h and β_r that appear in the scaling relations $BH = \tau^{\beta_h}$ and $SR = \tau^{\beta_r}$ [24]. Figure 5 shows the evolution of these two quantities for a particular set of parameters and the associated exponents. Simulations for different values of $\bar{F}$, $\bar{\kappa}$, and Θ show small variations in the exponents, in the ranges $\beta_h = 0.47 \pm 0.04$ and $\beta_r = 0.54 \pm 0.04$. The agreement with the experimental exponents $\beta_h = 0.49 \pm 0.09$ and $\beta_r = 0.50 \pm 0.09$ obtained by Omi *et al.* at 750 °C indicates that the combined dynamics-chemical effect captures bunching on Si(111) at this temperature without recourse to the inverse Schwoebel effect. Note that the latter provides, in the quasistatic approximation, comparable scaling exponents.

In summary, we have shown that dynamics can trigger bunching, even in the regime of very slow deposition, thus challenging the quasistatic approximation that prevails in the existing literature on step instabilities. When combined with the chemical effect (which is inherent to the driving force behind step motion but remains mostly unnaccounted for), it can quantitatively explain step bunching without recourse to the inverse ES barrier, whose existence remains controversial, or step-edge diffusion. When adequate parameters are chosen, the proposed model furnishes a plausible scenario for the onset of the bunching instability observed in Si(111)-(7×7) and GaAs(001). Further, our simulations of the moving boundary problem beyond the linear-stability regime confirm the formation and growth of step bunches in the presence of symmetric adatom attachment-detachment. Finally, the size-scaling analysis of the bunch patterns reveals that the combined chemical-dynamics effect can capture the bunching observed on Si(111)-(7×7) at 750 °C. Measurements of bunch patterns on material surfaces such as GaAs(001), for which evidence points to a direct ES barrier, would help to further validate the implication of the combined dynamics-chemical effect.

This work is supported by the "IDI 2015" project funded by the IDEX Paris-Saclay under ANR-11-IDEX-0003-02.

[1] T. Michely and J. Krug, *Islands, Mounds and Atoms* (Springer-Verlag Berlin Heidelberg, New York, 2004), Vol. 42, https://doi.org/10.1007/978-3-642-18672-1.
[2] R. L. Schwoebel and E. J. Shipsey, J. Appl. Phys. **37**, 3682 (1966).
[3] R. L. Schwoebel, J. Appl. Phys. **40**, 614 (1969).
[4] A. Pimpinelli and A. Videcoq, Surf. Sci. **445**, L23 (2000).
[5] M. Vladimirova, A. De Vita, and A. Pimpinelli, Phys. Rev. B **64**, 245420 (2001).
[6] P. Politi and J. Krug, Surf. Sci. **446**, 89 (2000).
[7] R. Ghez, H. G. Cohen, and J. B. Keller, J. Appl. Phys. **73**, 3685 (1993).
[8] F. Gillet, Ph.D. thesis, Université Joseph Fourier, Grenoble, France, 2000, https://www.theses.fr/2000GRE10204.
[9] B. Ranguelov and S. Stoyanov, Phys. Rev. B **76**, 035443 (2007).
[10] G. S. Bales and A. Zangwill, Phys. Rev. B **41**, 5500 (1990).
[11] A. Pimpinelli, I. Elkinani, A. Karma, C. Misbah, and J. Villain, J. Phys. Condens. Matter **6**, 2661 (1994).
[12] S. Stoyanov and V. Tonchev, Phys. Rev. B **58**, 1590 (1998).
[13] M. Sato, M. Uwaha, and Y. Saito, Phys. Rev. B **62**, 8452 (2000).
[14] O. Pierre-Louis, Surf. Sci. **529**, 114 (2003).
[15] O. Pierre-Louis and J.-J. Métois, Phys. Rev. Lett. **93**, 165901 (2004).
[16] R. Ghez and S. S. Iyer, IBM J. Res. Dev. **32**, 804 (1988).
[17] J. Krug, in *Multiscale Modeling in Epitaxial Growth*, edited by A. Voigt (Birkhäuser Basel, Basel, 2005), pp. 69–95, https://doi.org/10.1007/b137679.
[18] M. Kasu and T. Fukui, Jpn. J. Appl. Phys. **31**, L864 (1992).
[19] K. Hata, A. Kawazu, T. Okano, T. Ueda, and M. Akiyama, Appl. Phys. Lett. **63**, 1625 (1993).
[20] J. Ishizaki, S. Goto, M. Kishida, T. Fukui, and H. Hasegawa, Jpn. J. Appl. Phys. **33**, 721 (1994).
[21] K. Pond, J. Vac. Sci. Technol. B **12**, 2689 (1994).
[22] M. Shinohara and N. Inoue, Appl. Phys. Lett. **66**, 1936 (1995).
[23] J. Ishizaki, K. Ohkuri, and T. Fukui, Jpn. J. Appl. Phys. **35**, 1280 (1996).
[24] H. Omi, Y. Homma, V. Tonchev, and A. Pimpinelli, Phys. Rev. Lett. **95**, 216101 (2005).
[25] L. Guin, Ph.D. thesis, Université Paris-Saclay Ecole polytechnique, 2018, https://www.theses.fr/2018SACLX105.
[26] M. E. Jabbour, J. Elast. **80**, 153 (2005).
[27] P. Cermelli and M. Jabbour, Proc. R. Soc. A **461**, 3483 (2005).
[28] M. Dufay, T. Frisch, and J.-M. Debierre, Phys. Rev. B **75**, 241304 (2007).
[29] M. A. Załuska-Kotur and F. Krzyżewski, J. Appl. Phys. **111**, 114311 (2012).
[30] S. Chandrasekhar, *Hydrodynamic and Hydromagnetic Stability* (Dover, New York, 1981).
[31] R. Peyret, *Spectral Methods for Incompressible Viscous Flow* (Springer-Verlag, New York, 2002), Vol. 148, https://doi.org/10.1007/978-1-4757-6557-1.
[32] M. D. Johnson, K. T. Leung, A. Birch, and B. G. Orr, J. Cryst. Growth **174**, 572 (1997).
[33] J. Tersoff, M. D. Johnson, and B. G. Orr, Phys. Rev. Lett. **78**, 282 (1997).
[34] B. Voigtlander, A. Zinner, T. Weber, and H. P. Bonzel, Phys. Rev. B **51**, 7583 (1995).
[35] D. I. Rogilo, L. I. Fedina, S. S. Kosolobov, B. S. Ranguelov, and A. V. Latyshev, Phys. Rev. Lett. **111**, 036105 (2013).
[36] A. Ichimiya, Y. Tanaka, and K. Ishiyama, Phys. Rev. Lett. **76**, 4721 (1996).
[37] W. F. Chung and M. S. Altman, Phys. Rev. B **66**, 075338 (2002).
[38] J. Krug, Adv. Phys. **46**, 139 (1997).
[39] J. Stewart, O. Pohland, and J. M. Gibson, Phys. Rev. B **49**, 13848 (1994).
[40] R. Magri, S. K. Gupta, and M. Rosini, Phys. Rev. B **90**, 115314 (2014).
[41] R. Magri, S. K. Gupta, and M. Rosini, Phys. Rev. B **94**, 239909 (2016).
[42] J. H. Neave, P. J. Dobson, B. A. Joyce, and J. Zhang, Appl. Phys. Lett. **47**, 100 (1985).

[43] J. M. Van Hove and P. I. Cohen, J. Cryst. Growth **81**, 13 (1987).

[44] See the Supplemental Material at http://link.aps.org/supplemental/10.1103/PhysRevLett.124.036101 for details of the linear-stability analysis, the numerical resolution of the nonlinear step-flow equations, and the stability results for GaAs(001).

[45] A. Pimpinelli, V. Tonchev, A. Videcoq, and M. Vladimirova, Phys. Rev. Lett. **88**, 206103 (2002).

[46] J. Krug, V. Tonchev, S. Stoyanov, and A. Pimpinelli, Phys. Rev. B **71**, 045412 (2005).

[47] F. Krzyżewski, M. Załuska-Kotur, A. Krasteva, H. Popova, and V. Tonchev, Cryst. Growth Des. **19**, 821 (2019).

Supplemental material: Stability of vicinal surfaces: beyond the quasistatic approximation

L. Guin,[1,2] M. E. Jabbour,[1,3] L. Shaabani–Ardali,[4,5] L. Benoit–Maréchal,[1,2] and N. Triantafyllidis[1,3,6]

[1]*LMS, École polytechnique, CNRS, Institut polytechnique de Paris, 91128 Palaiseau, France*
[2]*LPICM, École polytechnique, CNRS, Institut polytechnique de Paris, 91128 Palaiseau, France*
[3]*Département de Mécanique, École polytechnique, 91128 Palaiseau, France*
[4]*LadHyX, École polytechnique, CNRS, Institut polytechnique de Paris, 91128 Palaiseau, France*
[5]*DAAA, ONERA, Université Paris-Saclay, F-92190 Meudon, France*
[6]*Aerospace Engineering Department & Mechanical Engineering Department (emeritus), The University of Michigan, Ann Arbor, Michigan 48109-2140, USA*

(Dated: November 11, 2019)

I. MATHEMATICAL DETAILS OF THE LINEAR STABILITY ANALYSIS

In this section, we provide the details of the derivation of the generalized eigenvalue problem Eq. (9) of the main text.

A. Mapping of the governing equations onto (0,1)

Using the relations between the partial derivatives of ρ_n and of $\tilde{\rho}_n$, we get

$$\begin{cases} \partial_t\tilde{\rho}_n = \big(\dot{x}_n + (\dot{x}_{n+1}-\dot{x}_n)u\big)\partial_x\rho_n + \partial_t\rho_n, \\ \partial_u\tilde{\rho}_n = (x_{n+1}-x_n)\partial_x\rho_n, \\ \partial_{uu}\tilde{\rho}_n = (x_{n+1}-x_n)^2\partial_{xx}\rho_n. \end{cases} \tag{S1}$$

We then rewrite the step dynamics governing equations (1)–(4) as

$$\begin{cases} s_n^2\partial_t\tilde{\rho}_n = \partial_{uu}\tilde{\rho}_n + s_n\big(\dot{x}_n + (\dot{x}_{n+1}-\dot{x}_n)u\big)\partial_u\tilde{\rho}_n + s_n^2\big(-\overline{\nu}\tilde{\rho}_n + \overline{F}\big), \\ -s_n\tilde{\rho}_n^-\dot{x}_{n+1} - (\partial_u\tilde{\rho}_n)^- = s_n\tilde{J}_{n+1}^-, \\ s_n\tilde{\rho}_n^+\dot{x}_n + (\partial_u\tilde{\rho}_n)^+ = s_n\tilde{J}_n^+, \\ \dot{x}_n = \Theta(\tilde{J}_n^+ + \tilde{J}_n^-), \end{cases} \tag{S2}$$

with $\tilde{J}_n^-$ and $\tilde{J}_n^+$ given by

$$\begin{cases} \tilde{J}_n^- = \overline{\kappa}\big(\tilde{\rho}_{n-1}^- - 1 - \Theta(\tilde{\rho}_n^+ - \tilde{\rho}_{n-1}^-) + f_n\big), \\ \tilde{J}_n^+ = \overline{\kappa}S\big(\tilde{\rho}_n^+ - 1 - \Theta(\tilde{\rho}_n^+ - \tilde{\rho}_{n-1}^-) + f_n\big), \end{cases} \tag{S3}$$

where $s_n := x_{n+1}-x_n$ and the superscripts plus and minus denote values at 0 and 1, respectively. Hence, $\tilde{\rho}_n^+ := \tilde{\rho}_n(0,t)$, $\tilde{\rho}_n^- := \tilde{\rho}_n(1,t)$, $(\partial_u\tilde{\rho}_n)^+ := \partial_u\tilde{\rho}_n(0,t)$ and $(\partial_u\tilde{\rho}_n)^- := \partial_u\tilde{\rho}_n(1,t)$. Note that the partial differential equation $(\text{S2})_1$ is defined on $(0,1)$.

B. Linear perturbation equation

Noting that for the steady-state solution the variable u coincides with the variable $x - x_n^*(t)$, the Lagrangian form of the principal solution reads $\tilde{\rho}^*(u) = \rho^*(u)$. To derive the linear perturbation equation, we consider the perturbed state

$$\begin{cases} x_n(t) = n + V^*t + \varepsilon\delta x_n(t) + o(\varepsilon), \\ \tilde{\rho}_n(u,t) = \tilde{\rho}^*(u) + \varepsilon\delta\tilde{\rho}_n(u,t) + o(\varepsilon), \end{cases} \tag{S4}$$

where ε is a small parameter and the perturbation is given by

$$\mathbf{q}_n(u,t) := \big(\delta x_n(t), \delta\tilde{\rho}_n(u,t)\big). \tag{S5}$$

Inserting (S4) in (S2) and collecting all terms of order ε yields a linear system for $\mathbf{q}_n$, which can be expressed in abstract form as

$$\mathcal{A}\big(\mathbf{q}_{n-1}, \mathbf{q}_n, \mathbf{q}_{n+1}, \mathbf{q}_{n+2}\big) = \mathcal{B}\big(\partial_t \mathbf{q}_n, \partial_t \mathbf{q}_{n+1}\big), \tag{S6}$$

where $\mathcal{A}$ and $\mathcal{B}$ denote the linear operators whose complete expressions are:

$$\begin{aligned}\mathcal{A}\big(\mathbf{q}_{n-1}, \mathbf{q}_n, \mathbf{q}_{n+1}, \mathbf{q}_{n+2}\big) = \\ \begin{pmatrix} A_1^1(u)\,(\delta x_n - \delta x_{n+1}) \\ A_2^1\,\delta x_n + A_2^{1\prime}\,\delta x_{n+1} + A_2^{1\prime\prime}\,\delta x_{n+2} \\ A_3^1\,\delta x_{n-1} + A_3^{1\prime}\,\delta x_n + A_3^{1\prime\prime}\,\delta x_{n+1} \\ A_4^1\,(\delta x_{n-1} - 2\delta x_n + \delta x_{n+1}) \end{pmatrix} + \begin{pmatrix} A_1^2\,\delta\tilde{\rho}_n(u,t) \\ A_2^2\,\delta\tilde{\rho}_{n+1}^+ + A_2^{2\prime}\,\delta\tilde{\rho}_n^- \\ A_3^2\,\delta\tilde{\rho}_n^+ + A_3^{2\prime}\,\delta\tilde{\rho}_{n-1}^- \\ A_4^2\,\delta\tilde{\rho}_n^+ + A_4^{2\prime}\,\delta\tilde{\rho}_{n-1}^- \end{pmatrix} + \begin{pmatrix} V^*\,\partial_u\delta\tilde{\rho}_n(u,t) \\ (\partial_u\delta\tilde{\rho}_n)^- \\ -(\partial_u\delta\tilde{\rho}_n)^+ \\ 0 \end{pmatrix} + \begin{pmatrix} \partial_{uu}\delta\tilde{\rho}_n(u,t) \\ 0 \\ 0 \\ 0 \end{pmatrix}, \end{aligned} \tag{S7}$$

with

$$\begin{cases} A_1^1(u) = 2\nu\rho^*(u) - 2F - V^*\rho^{*\prime}(u), \qquad A_2^1 = \overline{\kappa}(1+3\overline{\alpha}) + \overline{\kappa}\Theta\rho^*(0) - \big(\overline{\kappa}(1+\Theta) + V^*\big)\rho^*(1), \\ A_2^{1\prime} = -\overline{\kappa}(1+6\overline{\alpha}) - \overline{\kappa}\Theta\rho^*(0) + \big(\overline{\kappa}(1+\Theta) + V^*\big)\rho^*(1), \qquad A_2^{1\prime\prime} = 3\overline{\kappa\alpha}, \qquad A_3^1 = 3S\overline{\kappa\alpha}, \\ A_3^{1\prime} = \overline{\kappa}S(1-6\overline{\alpha}) - \overline{\kappa}S\Theta\rho^*(1) + \big(\overline{\kappa}S + \Theta - 1 + V^*\big)\rho^*(0), \\ A_3^{1\prime\prime} = -\overline{\kappa}S(1-3\overline{\alpha}) + \overline{\kappa}S\Theta\rho^*(1) + \big(\overline{\kappa}S + 1 - \Theta - V^*\big)\rho^*(0), \\ A_4^1 = -3\Theta\overline{\kappa\alpha}(1+S), \qquad A_1^2 = -\overline{\nu}, \qquad A_2^2 = -\overline{\kappa}\Theta, \quad A_2^{2\prime} = \overline{\kappa}(1+\Theta) + V^*, \\ A_3^2 = \overline{\kappa}S(1-\Theta) - V^*, \qquad A_3^{2\prime} = \Theta\overline{\kappa}S, \qquad A_4^2 = \Theta\overline{\kappa}\big(\Theta(1+S) - S\big), \qquad A_4^{2\prime} = -\Theta\overline{\kappa}\big(\Theta(1+S) + 1\big). \end{cases} \tag{S8}$$

where $\rho^{*\prime}$ denotes the first derivative of ρ^* and

$$\mathcal{B}\big(\partial_t\mathbf{q}_n, \partial_t\mathbf{q}_{n+1}\big) = \begin{pmatrix} (u-1)\rho^{*\prime}(u)\delta\dot{x}_n - u\rho^{*\prime}(u)\delta\dot{x}_{n+1} + \partial_t\delta\tilde{\rho}_n(u,t) \\ \rho^*(1)\delta\dot{x}_{n+1} \\ \rho^*(0)\delta\dot{x}_n \\ \delta\dot{x}_n \end{pmatrix}. \tag{S9}$$

C. Floquet-mode analysis

Using the linearity of (S6) and noting that the operators $\mathcal{A}$ and $\mathcal{B}$ are time independent and independent of n (i.e., invariant under a one-terrace translation), the perturbations that solve (S6) can be written as combinations of normal *Floquet modes*:

$$\begin{cases} \delta x_n(t) = \delta\hat{x}\exp(ikn + \lambda t), \\ \delta\tilde{\rho}_n(u,t) = \delta\hat{\rho}(u)\exp(ikn + \lambda t), \end{cases} \tag{S10}$$

with i the imaginary unit, $k \in (-\pi, \pi)$ the wave number and λ the associated growth rate. Hence, the stability of the system is obtained from the stability of each one of the modes.

Inserting (S10) in (S6) yields, for a given wavenumber k, a generalized eigenvalue problem of the form

$$\hat{\mathcal{A}}_k\hat{\mathbf{q}} = \lambda\hat{\mathcal{B}}_k\hat{\mathbf{q}}, \tag{S11}$$

where $\hat{\mathbf{q}}(u) := \big(\delta\hat{x}, \delta\hat{\rho}(u)\big)$ and $\hat{\mathcal{A}}_k$ and $\hat{\mathcal{B}}_k$ are linear operators deriving from $\mathcal{A}$ and $\mathcal{B}$, whose complete expressions are:

$$\hat{\mathcal{A}}_k\hat{\mathbf{q}} = \begin{pmatrix} \hat{A}_1^1(u)\delta\hat{x} \\ \hat{A}_2^1\,\delta\hat{x} \\ \hat{A}_3^1\,\delta\hat{x} \\ \hat{A}_4^1\,\delta\hat{x} \end{pmatrix} + \begin{pmatrix} \hat{A}_1^2\,\delta\hat{\rho}(u) \\ \hat{A}_2^2\,\delta\hat{\rho}(0) + \hat{A}_2^{2\prime}\,\delta\hat{\rho}(1) \\ \hat{A}_3^2\,\delta\hat{\rho}(0) + \hat{A}_3^{2\prime}\,\delta\hat{\rho}(1) \\ \hat{A}_4^2\,\delta\hat{\rho}(0) + \hat{A}_4^{2\prime}\,\delta\hat{\rho}(1) \end{pmatrix} + \begin{pmatrix} V^*\,\delta\hat{\rho}'(u) \\ \delta\hat{\rho}'(1) \\ -\delta\hat{\rho}'(0) \\ 0 \end{pmatrix} + \begin{pmatrix} \delta\hat{\rho}''(u) \\ 0 \\ 0 \\ 0 \end{pmatrix}, \tag{S12}$$

where $\delta\hat{\rho}'$ and $\delta\hat{\rho}''$ denote the first and second derivatives of $\delta\hat{\rho}$, respectively and

$$\hat{\mathcal{B}}_k\hat{\mathbf{q}} = \begin{pmatrix} \hat{B}_1^1(u)\delta\hat{x} \\ \hat{B}_2^1\,\delta\hat{x} \\ \hat{B}_3^1\,\delta\hat{x} \\ -\delta\hat{x} \end{pmatrix} + \begin{pmatrix} \delta\hat{\rho}(u) \\ 0 \\ 0 \\ 0 \end{pmatrix}, \tag{S13}$$

with

$$\begin{cases} \hat{A}_1^1(u) = \left(-1+\mathrm{e}^{ik}\right)\left(2\overline{F} - 2\overline{\nu}\rho^*(u) + V^*\rho^{*\prime}(u)\right), \\ \hat{A}_2^1 = \left(-1+\mathrm{e}^{ik}\right)\Big(\overline{\kappa}\left(3(\mathrm{e}^{ik}-1)\overline{\alpha} + (\rho^*(1)-\rho^*(0))\Theta + \rho^*(1) - 1\right) + V^*\rho^*(1)\Big), \\ \hat{A}_3^1 = \left(-1+\mathrm{e}^{ik}\right)\Big(3\overline{\kappa}S\left((1-\mathrm{e}^{-ik})\overline{\alpha} - \rho^*(0)(\Theta-1) + \rho^*(1)\Theta - 1\right) - V^*\rho^*(0)\Big), \\ \hat{A}_4^1 = -6\Theta\overline{\kappa}\overline{\alpha}(S+1)(\cos(k)-1), \\ \hat{A}_1^2 = -\overline{\nu}, \quad \hat{A}_2^2 = -\mathrm{e}^{ik}\overline{\kappa}\Theta, \quad \hat{A}_2^{2\prime} = \overline{\kappa}(1+\Theta) + V^*, \\ \hat{A}_3^2 = \overline{\kappa}S(1-\Theta) - V^*, \quad \hat{A}_3^{2\prime} = \mathrm{e}^{-ik}\Theta\overline{\kappa}S, \\ \hat{A}_4^2 = \Theta\overline{\kappa}\big((S+1)\Theta - S\big), \quad \hat{A}_4^{2\prime} = -\mathrm{e}^{-ik}\Theta\overline{\kappa}\big((S+1)\Theta + 1\big), \\ \hat{B}_1^1(u) = -\left(1 + \left(-1+\mathrm{e}^{ik}\right)u\right)\rho^{*\prime}(u), \quad \hat{B}_2^1 = -\mathrm{e}^{ik}\hat{\rho}^*(1), \quad \hat{B}_3^1 = \hat{\rho}^*(0). \end{cases} \tag{S14}$$

The numerical resolution of (S11) for a given k provides the set of associated eigenvalues (whose number depends on the numerical mesh resolution). The eigenvalue corresponding to the most unstable mode is the one with largest real part.

Note that as the operators $\hat{\mathcal{A}}_{-k}$ and $\hat{\mathcal{B}}_{-k}$ are the complex conjugates of $\hat{\mathcal{A}}_k$ and $\hat{\mathcal{B}}_k$, respectively, the eigenvalues associated with the wavelength $-k$ are complex conjugate to those of wavelength k. As a result, the set of eigenvalues of wavelength $-k$ and k have the same real part, which allows us to reduce the computation of the growth rate $\mathrm{Re}(\lambda)[k]$ to $k \in (0,\pi)$, interval over which the dispersion relations are displayed (see, e.g., Fig. 2 of the main text).

II. LINEAR STABILITY RESULTS FOR GAAS(001)

We report in Fig.S1 the stability diagram obtained from representative physical parameters for GaAs(001).

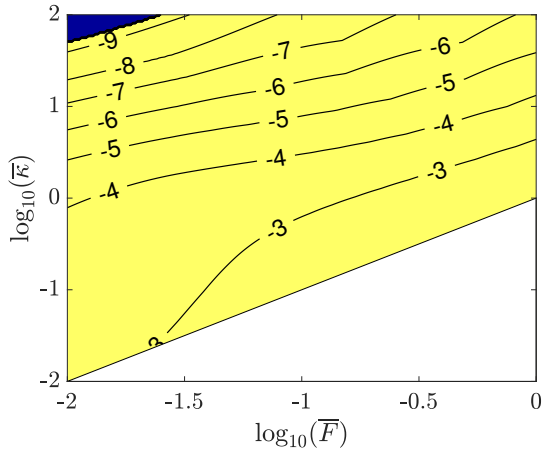

FIG. S1. Stability diagram for the deposition of GaAs(001), with $\overline{\nu} = 0$, $\Theta = 0.2$, $S = 2$, $\overline{\alpha} = 5 \times 10^{-6}$. Blue (dark) and yellow (light) correspond to the stable and unstable domains, and isolines display $\max_{k\in(-\pi,\pi)} \log_{10} \mathrm{Re}(\lambda)$. The white area corresponds to a unphysical domain where the adatom density reaches values well above the equilibrium adatom coverage.

The choice of value for each parameter is explained in the main text. We can see the existence in Fig. S1 of an unstable domain, quantitatively important for low values of $\overline{\kappa}$. Specifically, for $\overline{\kappa} < 1$ the observed instability develops in 10 to 100 monolayers, which is fast enough to account for the bunching observed in the experiments mentioned in

the main text. It should be noted that this unstable domain depends strongly on the strength of the ES barrier and disappears when it is larger than $S = 2$.

III. NUMERICAL RESOLUTION OF THE FULLY NON-LINEAR STEP FLOW EVOLUTION PROBLEM

In this section, we present the numerical scheme developed to solve the moving boundary problem of step flow, which furnishes, beyond the onset of the bunching instability, the growth of step bunches. As step bunches grow in time, the adatom density on terraces presents large deviations from its equilibrium value and the assumption of *near-equilibrium adatom density* ($|\rho - 1| \ll 1$, in dimensionless form) underlying the linear step-flow problem, as formulated in Equations (1)–(4) of the main text, is no longer valid. Therefore, to compute bunch growth, we resort to the nonlinear step-flow evolution problem from which (1)-(4) derives [S1, S2]. In the absence of evaporation, the moving boundary problem reads

$$\begin{cases} \partial_t \rho_n = \partial_{xx}\rho_n + \bar{F}, \\ -\rho_n^- \dot{x}_{n+1} - (\partial_x \rho_n)^- = J_{n+1}^-, \\ \rho_n^+ \dot{x}_n + (\partial_x \rho_n)^+ = J_n^+, \\ \dot{x}_n = \Theta(J_n^+ + J_n^-), \end{cases} \tag{S15}$$

where J_n^- and J_n^+ are given by

$$\begin{cases} J_n^- = \bar{\kappa}\left(\ln(\rho_{n-1}^-) - \Theta(\rho_n^+ - \rho_{n-1}^-) + f_n\right), \\ J_n^+ = \bar{\kappa} S\left(\ln(\rho_n^+) - \Theta(\rho_n^+ - \rho_{n-1}^-) + f_n\right). \end{cases} \tag{S16}$$

Further, to deal with the moving steps, we rewrite the system in a Lagrangian form with the change of space variable from x to u and the associated change of adatom density from ρ_n to $\tilde{\rho}_n$ given in (6) of the main text and detailed in Section I A above. This leads to the Lagrangian nonlinear adatom density evolution problem:

$$\begin{cases} s_n^2 \partial_t \tilde{\rho}_n = \partial_{uu}\tilde{\rho}_n + s_n\big(\dot{x}_n + (\dot{x}_{n+1} - \dot{x}_n)u\big)\partial_u \tilde{\rho}_n + s_n^2 \bar{F}, \\ -s_n \tilde{\rho}_n^- \dot{x}_{n+1} - (\partial_u \tilde{\rho}_n)^- = s_n \tilde{J}_{n+1}^-, \\ s_n \tilde{\rho}_n^+ \dot{x}_n + (\partial_u \tilde{\rho}_n)^+ = s_n \tilde{J}_n^+, \\ \dot{x}_n = \Theta(\tilde{J}_n^+ + \tilde{J}_n^-), \end{cases} \tag{S17}$$

where $\tilde{J}_n^-$ and $\tilde{J}_n^+$ take the form

$$\begin{cases} \tilde{J}_n^- = \bar{\kappa}(\ln(\tilde{\rho}_{n-1}^-) - \Theta(\tilde{\rho}_n^+ - \tilde{\rho}_{n-1}^-) + f_n), \\ \tilde{J}_n^+ = \bar{\kappa} S(\ln(\tilde{\rho}_n^+) - \Theta(\tilde{\rho}_n^+ - \tilde{\rho}_{n-1}^-) + f_n). \end{cases} \tag{S18}$$

Note that in (S17)-(S18), the functions $\tilde{\rho}_n(\cdot, t)$ are defined on $(0, 1)$ and the variables $x_n(t)$, while no longer being the boundaries of the domains over which the differential equations are resolved, furnish the step positions.

The numerical resolution is performed on a system of $N = 500$ steps, with periodic boundary conditions, where each terrace is discretized using the finite element method with second-order interpolation functions, 3-point Gauss quadrature, and one element. Indeed, the parabolic profile for the adatom concentration on terraces for stable equidistant step flow suggests that a unique element per terrace is sufficient. Further, we observe no noticeable mesh-dependence when increasing the terrace discretization up to ten elements per terrace. For the time-evolution problem, we use an implicit solver implementing a variable-step, variable-order scheme.

The surface roughness of a sample of length L whose height is described by the function $h(x)$ (with average $\overline{h} := \frac{1}{L}\int_0^L h(x)\mathrm{d}x$) is defined as

$$SR = \sqrt{\frac{1}{L}\int_0^L \left[h(x) - \overline{h}\right]^2 \mathrm{d}x}. \tag{S19}$$

Denoting by a the step height and $\{x_n\}_{1\leq n\leq N}$ the step positions, the roughness of the vicinal surface reads

$$SR = a\sqrt{\frac{1}{3N}\sum_{n=1}^{N}\left\{\left(x_{n+1}-n+\frac{1}{2}\right)^3-\left(x_n-n+\frac{1}{2}\right)^3\right\}}. \tag{S20}$$

For computing the median bunch height, a step is considered to belong to a bunch when its distance to the neighboring steps is below 0.2. Note that the value of this threshold has very little influence on the resulting median bunch height.

Finally, the exponents β_h and β_r defined in the main text are computed through a linear regression in log-log scale, after cutting off the initial transient regime, cf. Fig. 5.

[S1] P. Cermelli and M. Jabbour, Proceedings of the Royal Society of London A: Mathematical, Physical and Engineering Sciences **461**, 3483 (2005).

[S2] L. Guin, *Electromechanical couplings and growth instabilities in semiconductors*, Ph.D. thesis, Université Paris-Saclay - Ecole polytechnique (2018).